Color-flavor reflection in the continuum limit of two-dimensional lattice gauge theories with scalar fields

Claudio Bonati and Alessio Franchi ⓞ

Dipartimento di Fisica dell'Università di Pisa and INFN, Largo Pontecorvo 3, I-56127 Pisa, Italy

We address the interplay between local and global symmetries in determining the continuum limit of two-dimensional lattice scalar theories characterized by SO(N_c) gauge symmetry and non-Abelian O(N_f) global invariance. We argue that, when a quartic interaction is present, the continuum limit of these models corresponds in some cases to the gauged nonlinear σ model field theory associated with the real Grassmannian manifold SO(N_f)/(SO(N_c) × SO($N_f - N_c$)), which is characterized by the invariance under the color-flavor reflection $N_c \leftrightarrow N_f - N_c$. Monte Carlo simulations and finite-size scaling analyses, performed for $N_f = 7$ and several values of N_c, confirm the emergence of the color-flavor reflection symmetry in the scaling limit and support the identification of the continuum limit.

I. INTRODUCTION

Global and local symmetries are cornerstones of our understanding of many different physical phenomena, ranging from high energy physics to many-body systems in condensed-matter physics [1,2]. Global symmetries characterize fundamental features of a physical model, like its phase diagram and energy spectrum [3]. Gauge symmetries, instead, constrain the form of the possible interactions, are responsible for the presence of Higgs phases, and are necessary to describe some emergent phenomena in condensed-matter systems [4,5].

The nature of the interplay between local and global symmetries at a phase transition is a long-standing issue [6–10], which, however, is still not completely clarified. Two-dimensional scalar models with local and global symmetries are perfect playgrounds to investigate this topic, since their critical properties can be studied by means of numerical simulations requiring only a moderate computational effort. In particular, recent works have considered two-dimensional scalar models with orthogonal local symmetries [11,12] and models with unitary local symmetries and scalar matter transforming in different representations of the gauge group [13,14].

According to the Mermin-Wagner theorem [15], in two-dimensional systems the critical behavior associated with the breaking of a continuous global symmetry can be observed only in the zero-temperature limit. This obviously remains true also for gauge models, but in this case two different classes of low-temperature behavior can *a priori* be expected to emerge, depending whether the gauge degrees of freedom are or are not critical at the transition.

For most of the two-dimensional gauge models studied so far (see, e.g., Refs. [11–13]), gauge degrees of freedom do not develop long-range correlations at the transition. In these cases gauge symmetry does not seem to play a pivotal role in determining the low-temperature universal critical behavior: the size of the gauge group (i.e., N_c) does not influence the critical low-temperature regime, just like the specific matter field representation. Also in this case, however, gauge symmetry plays in fact a fundamental role: that of selecting the critical degrees of freedom, preventing non-gauge-invariant observables from developing critical correlations. Gauge fields are instead expected to become critical for some values of the parameters of the model studied in Ref. [14], where this fact was attributed to the presence of quartic scalar field interactions (see Refs. [16–18] for the analogous three-dimensional case).

The aim of this paper is to extend the results of Refs. [11,14] by studying a lattice model characterized by SO(N_c) local invariance, multicomponent scalar fields transforming in the fundamental representation of the color group, and non-Abelian O(N_f) global symmetry together with a quartic interaction. This field content is indeed better suited than the one used in Ref. [14] to investigate a peculiar symmetry between N_c and N_f, that we expect to emerge in the continuum limit. The origin of this symmetry is the following: we will argue the continuum limit of the model studied in this paper to be (at least in some regions of the parameter space) the nonlinear σ model (NLσM) field theory associated with the Grassmannian manifold SO(N_f)/(SO(N_c) × SO($N_f - N_c$)). Since this manifold is clearly invariant under the exchange $N_c \leftrightarrow N_f - N_c$, we expect this "color-flavor reflection symmetry" to characterize also the low-temperature critical behavior of the gauge model. A numerical verification of the emergence of this symmetry will strongly support the identification of the continuum limit with the Grassmann NLσM field theory.

The paper is organized as follows: In Sec. II we present the lattice model. In Sec. III we discuss its minimum-energy configurations controlled by the quartic interaction and identify the different continuum limits exhibited by the lattice

model in the space of parameters. In Sec. IV we introduce the observables and the finite-size scaling (FSS) theory used in actual numerical analyses. In Sec. V we present our numerical results, in Sec. VI we finally draw our conclusions and present possible outlooks of our work. Some technical details concerning the algorithms and the Monte Carlo simulations are reported in the Appendix.

II. THE LATTICE MODEL

The matter field of the lattice model studied in this work is a multicomponent real scalar field $\Phi_{\boldsymbol{x}}^{i\alpha}$, where $i = 1, \ldots, N_c$ and $\alpha = 1, \ldots, N_f$ stand for the "color" and the "flavor" indices, respectively, and $\boldsymbol{x} = (x_1, x_2)$ denotes the position on the lattice. For the sake of simplicity we will adopt the unit-length (London limit) constraint $\mathrm{Tr}\Phi_{\boldsymbol{x}}^t\Phi_{\boldsymbol{x}} = 1$, which is not expected to alter the critical behavior of the model.

To define the lattice Hamiltonian, we start from the most general quartic interaction for the field $\Phi^{i\alpha}$ compatible with the $\mathrm{O}(N_c) \times \mathrm{O}(N_f)$ global invariance, i.e., from the lattice NLσM with Hamiltonian

$$H_\sigma = -N_f \sum_{\boldsymbol{x}, \mu > 0} \mathrm{Tr}\Phi_{\boldsymbol{x}}^t\Phi_{\boldsymbol{x}+\hat{\mu}} + w \sum_{\boldsymbol{x}} \mathrm{Tr}\Phi_{\boldsymbol{x}}^t\Phi_{\boldsymbol{x}}\Phi_{\boldsymbol{x}}^t\Phi_{\boldsymbol{x}}, \quad (1)$$

where $\hat{\mu} = \hat{1}, \hat{2}$ denotes a lattice vector, the coefficient of the first term has been normalized to N_f, and periodic boundary conditions in all directions are assumed. The lattice gauge model is obtained by gauging the color degrees of freedom of the matter field, coupling them to a link variable $U_{\boldsymbol{x},\mu} \in \mathrm{SO}(N_c)$ following Wilson's prescription [19].

The complete Hamiltonian can thus be written in the form

$$H = H_K(\Phi_{\boldsymbol{x}}, U_{\boldsymbol{x},\mu}) + V(\Phi_{\boldsymbol{x}}) + H_G(U_{\boldsymbol{x},\mu}). \quad (2)$$

In this expression $H_K(\Phi, U)$ and $V(\Phi)$ represent the scalar field kinetic energy and the quartic interaction, respectively, which are defined as follows:

$$H_K(\Phi_{\boldsymbol{x}}, U_{\boldsymbol{x},\mu}) = -N_f \sum_{\boldsymbol{x}, \mu > 0} \mathrm{Tr}\Phi_{\boldsymbol{x}}^t U_{\boldsymbol{x},\mu}\Phi_{\boldsymbol{x}+\hat{\mu}}, \quad (3)$$

$$V(\Phi_{\boldsymbol{x}}) = w \sum_{\boldsymbol{x}} \mathrm{Tr}\Phi_{\boldsymbol{x}}^t\Phi_{\boldsymbol{x}}\Phi_{\boldsymbol{x}}^t\Phi_{\boldsymbol{x}}. \quad (4)$$

The last term $H_G(U_{\boldsymbol{x},\mu})$ in Eq. (2) represents instead the kinetic term of the gauge field, and it is written by means of the plaquette operator Π_x in the usual Wilson form:

$$H_G(U_{\boldsymbol{x}}) = -\frac{\gamma}{N_c} \sum_{\boldsymbol{x}} \mathrm{Tr}\Pi_{\boldsymbol{x}}, \quad (5)$$

$$\Pi_{\boldsymbol{x}} = U_{\boldsymbol{x},1} U_{\boldsymbol{x}+\hat{1},2} U_{\boldsymbol{x}+\hat{2},1}^t U_{\boldsymbol{x},2}^t. \quad (6)$$

The model is characterized by a gauge $\mathrm{SO}(N_c)$ invariance under the local transformation

$$\Phi_{\boldsymbol{x}} \mapsto W_{\boldsymbol{x}}\Phi_{\boldsymbol{x}}, \quad U_{\boldsymbol{x},\mu} \mapsto W_{\boldsymbol{x}} U_{\boldsymbol{x},\mu} W_{\boldsymbol{x}+\hat{\mu}}^t, \quad (7)$$

where $W_{\boldsymbol{x}} \in \mathrm{SO}(N_c)$, and by a global $\mathrm{O}(N_f)$ invariance under $\Phi_{\boldsymbol{x}} \mapsto \Phi_{\boldsymbol{x}}M$, with $M \in \mathrm{O}(N_f)$. The partition function of the statistical model is finally defined by

$$Z = \sum_{\{\Phi, U\}} e^{-\beta H}, \quad (8)$$

where β plays the role of the inverse temperature.

The Hamiltonian in Eq. (2) has several limiting cases which correspond to known and already studied models. For $w = 0$ and $\gamma = \infty$ it trivially reduces to the standard $\mathrm{O}(N_cN_f)$ model, while for $w = 0$ and finite γ it reduces to the model studied in Ref. [11]. The case $N_c = 2$ for $w = 0$ is quite peculiar, since the global symmetry is not $\mathrm{O}(N_f)$ but $\mathrm{U}(N_f)$ (see Ref. [20]). Finally, as will be clear from the analysis of the minimum-energy configurations carried out in the next section, when $N_f > N_c$ the Hamiltonian reduces in the limit $w = \infty$ and $\gamma = \infty$ to that of the so-called Stiefel models, which are the NLσMs defined on the homogeneous spaces $\mathrm{SO}(N_f)/\mathrm{SO}(N_f - N_c)$ [21–23].

In this work we will mainly focus on the case $\gamma = 0$, as we do not expect the gauge coupling to play a relevant role at criticality in two dimensions (apart from crossover effects in the limit $\gamma \to \infty$), just as in all previously studied cases [11–14].

III. MINIMUM-ENERGY CONFIGURATIONS AND CONTINUUM LIMITS

In this section we identify the minimum-energy configurations of the gauge model in Eq. (2), which are expected to be the ones characterizing the low-temperature ($\beta \to +\infty$) critical behavior of the model. The minimum-energy configurations are selected by the quartic interaction, and their determination uses arguments that partially retrace those used in Refs. [14,18].

By means of the singular value decomposition, the scalar field matrix $\Phi_{\boldsymbol{x}}^{i\alpha}$ can be rewritten as follows:

$$\Phi_{\boldsymbol{x}}^{i\alpha} = \sum_{j=1}^{N_c} \sum_{\delta=1}^{N_f} C_{\boldsymbol{x}}^{ij} D_{\boldsymbol{x}}^{j\delta} F_{\boldsymbol{x}}^{\alpha\delta}, \quad (9)$$

where C and F are two square matrices in $\mathrm{O}(N_c)$ and $\mathrm{O}(N_f)$, respectively, $D = \mathrm{diag}\{s_1, \ldots, s_q\}$ is an $N_c \times N_f$ matrix with non-negative diagonal entries, and $q \equiv \min[N_c, N_f]$. The fixed-length constraint becomes

$$\mathrm{Tr}\Phi_{\boldsymbol{x}}^t\Phi_{\boldsymbol{x}} = \sum_{i=1}^{q} s_i^2 = 1, \quad (10)$$

and the the quartic potential term is equal to

$$\mathrm{Tr}\Phi_{\boldsymbol{x}}^t\Phi_{\boldsymbol{x}}\Phi_{\boldsymbol{x}}^t\Phi_{\boldsymbol{x}} = \sum_{i=1}^{q} s_i^4. \quad (11)$$

The explicit form of the minimum-energy configurations is fixed by the sign of the quartic coupling w:

(1) $s_1 = 1, s_2 = s_3 = \cdots = s_q = 0$ if $w < 0$.

(2) $s_1 = \cdots = s_q = 1/\sqrt{q}$ if $w > 0$.

The residual symmetry of these minima determines the low-temperature critical behavior of the model, which is thus expected to be different for positive or negative values of the coupling w. The case $w = 0$ requires special attention and, apart from a few cases in which analytical results can be obtained (see Refs. [14,18]), we have to rely on numerical simulations for the identification of the critical behavior when $w = 0$.

When configurations of type (i) dominate the partition function (i.e., for $w < 0$), the continuum limit is expected to

be the same as the $\mathbb{R}P^{N_f-1}$ model [11,14]. The simplest way to understand this fact is to note that, by using configurations of type (i), it is possible to construct the gauge-invariant composite field $B_{\boldsymbol{x}} = \Phi_{\boldsymbol{x}}^t \Phi_{\boldsymbol{x}}$, which behaves as a rank-1 real space projector (i.e., $B_{\boldsymbol{x}}^2 = B_{\boldsymbol{x}} = B_{\boldsymbol{x}}^t$ and $\mathrm{Tr} B_{\boldsymbol{x}} = 1$). Indeed the $\mathbb{R}P^{N_f-1}$ model describes the dynamics of a rank-1 projector $P_{\boldsymbol{x}}$ in an N_f-dimensional space. By introducing the unit-length vector $S_{\boldsymbol{x}}$ using the definition $P_{\boldsymbol{x}}^{\alpha\delta} = S_{\boldsymbol{x}}^\alpha S_{\boldsymbol{x}}^\delta$, the action of the $\mathbb{R}P^{N_f-1}$ model can be written as [24–27]

$$H_{RP} = -\sum_{\boldsymbol{x},\mu} \mathrm{Tr} P_{\boldsymbol{x}} P_{\boldsymbol{x}+\hat{\mu}} = -\sum_{\boldsymbol{x},\mu} (S_{\boldsymbol{x}} \cdot S_{\boldsymbol{x}+\hat{\mu}})^2, \qquad (12)$$

which displays the two main features of the $\mathbb{R}P^{N_f-1}$ universality class: $O(N_f)$ global invariance and $\mathbb{Z}_2$ local invariance. We thus expect the $SO(N_c)$ symmetry not to play any significant role in the continuum limit of the model for $w < 0$. Moreover, in Ref. [11] it was numerically shown that the same is also true for the case $w = 0$, and for all the values of γ investigated.

We can now discuss the case in which the dominant configurations are those of type (ii). Using an argument analogous to that used for the unitary groups in Ref. [18], it is possible to show that if $N_f \leqslant N_c$ there is no residual global symmetry for the field $\Phi_{\boldsymbol{x}}$ in this case; hence no critical behavior at all is expected in the low-temperature limit when $w > 0$ (see Ref. [14] for a numerical check). For this reason, in the following, we will assume $N_f > N_c$; hence $q = N_c$. As for the case of type (i) minima, it is convenient to introduce a gauge-invariant composite field, which is now $\widetilde{B}_{\boldsymbol{x}} = N_c \Phi_{\boldsymbol{x}}^t \Phi_{\boldsymbol{x}}$. It is indeed simple to show, using the explicit form of the type (ii) minima, that $\widetilde{B}_{\boldsymbol{x}}^2 = \widetilde{B}_{\boldsymbol{x}} = \widetilde{B}_{\boldsymbol{x}}^t$ and $\mathrm{Tr} \widetilde{B}_{\boldsymbol{x}} = N_c$; hence $\widetilde{B}_{\boldsymbol{x}}$ is a rank-N_c real space projector. The lattice NLσM written by using $\widetilde{B}_{\boldsymbol{x}}$, whose Hamiltonian is

$$H_G = -\sum_{\boldsymbol{x},\mu} \mathrm{Tr} \widetilde{B}_{\boldsymbol{x}} \widetilde{B}_{\boldsymbol{x}+\hat{\mu}}, \qquad (13)$$

is a possible discretization of the NLσM field theory associated with the real Grassmannian manifolds

$$SO(N_f)/(SO(N_c) \times SO(N_f - N_c)), \qquad (14)$$

where we have neglected discrete subgroups that, as usual, are not expected to play any role in the zero-temperature limit.

The same conclusion about the global symmetry breaking pattern for $w > 0$ can be reached also in another way, by using as an effective model the Hamiltonian $H_K(\Phi_{\boldsymbol{x}}, U_{\boldsymbol{x},\mu})$, with the field $\Phi_{\boldsymbol{x}}$ restricted to be of the form (ii). Introducing the rescaled field $\widetilde{\Phi}_{\boldsymbol{x}} = \sqrt{N_c} \Phi_{\boldsymbol{x}}$, the effective model Hamiltonian is written as

$$H_K^{w\to\infty} = -\frac{N_f}{N_c} \sum_{\boldsymbol{x},\mu} \mathrm{Tr} \widetilde{\Phi}_{\boldsymbol{x}}^t U_{\boldsymbol{x},\mu} \widetilde{\Phi}_{\boldsymbol{x}+\mu}. \qquad (15)$$

By using essentially the same arguments discussed in Ref. [18] for the unitary group case, one obtains again for the global invariance group of $H_K^{w\to\infty}$ the expression in Eq. (14) (again up to discrete groups).

Two-dimensional Grassmannian NLσM field theories have been introduced in Refs. [28,29], are known to be asymptotically free [3,29], and their β functions are known up to four loops in dimensional regularization [30]. Since Grassmann manifolds are invariant under the color-flavor reflection $N_c \leftrightarrow$

$N_f - N_c$, our study of the minimum-energy configurations leads us to expect this symmetry to emerge in the critical low-temperature behavior of the lattice model in Eq. (2) when $w > 0$. We explicitly note that this symmetry is present also when $w < 0$; however, in that case it is realized in a somehow trivial way: the critical behavior is expected to always be that of the $\mathbb{R}P^{N_f-1}$ model, for all N_c values. In Sec. V we will provide numerical evidence that, for $w > 0$, the universal FSS curves of the lattice model considered in this paper do depend on N_c and that the color-flavor reflection symmetry is realized.

We close this discussion by noting that the second approach used above to identify the invariance group when $w > 0$, and in particular the effective Hamiltonian in Eq. (15), is especially convenient to clarify the relation of the model we are studying with the Stiefel models. In the limit $\gamma \to \infty$ we have $U_{\boldsymbol{x},\mu} \to 1$ up to gauge transformations (at least in the thermodynamic limit). Moreover, it is immediate to verify that for type (ii) minima the following relation holds true:

$$\widetilde{\Phi}_{\boldsymbol{x}} \widetilde{\Phi}_{\boldsymbol{x}}^t = \mathbb{1}_{N_c \times N_c}, \qquad (16)$$

where $\mathbb{1}_{N_c \times N_c}$ denotes the $N_c \times N_c$ identity matrix (note that this relation is gauge invariant although color indices are not contracted). For $\gamma \to \infty$ the Hamiltonian $H_K^{w\to\infty}$ in Eq. (15) thus reduces, up to an irrelevant multiplicative factor that can be reabsorbed in the normalization of β, to that of the Stiefel model $V_{(N_f,N_c)}$, which is usually written as [21–23]

$$H_S = -N_f \sum_{\boldsymbol{x},\mu} \mathrm{Tr} \pi_{\boldsymbol{x}}^t \pi_{\boldsymbol{x}+\mu}, \qquad (17)$$

where $\pi_{\boldsymbol{x}}$ are $N_c \times N_f$ real matrices (with $N_f > N_c$) satisfying the constraints

$$\pi_{\boldsymbol{x}} \pi_{\boldsymbol{x}}^t = \mathbb{1}_{N_c \times N_c}. \qquad (18)$$

The continuum limit of this model is described by the NLσM field theory having the manifold $SO(N_f)/SO(N_f - N_c)$ as target space, and which is associated to the symmetry breaking pattern $SO(N_f) \to SO(N_f - N_c)$ (see, e.g., Ref. [21] for more details).

A summary graph of the different low-temperature behaviors expected on the basis of the residual symmetry of the minimum-energy configurations is shown in Fig. 1.

IV. OBSERVABLES AND FINITE-SIZE SCALING

To characterize the critical behavior of the lattice models we use Monte Carlo simulations and FSS techniques [31–33]. We focus on the bilinear local operator $Q_{\boldsymbol{x}}$,

$$B_{\boldsymbol{x}}^{\alpha\beta} = \sum_{i=1}^{N_c} \Phi_{\boldsymbol{x}}^{i\alpha} \Phi_{\boldsymbol{x}}^{i\beta}, \quad Q_{\boldsymbol{x}}^{\alpha\beta} = B_{\boldsymbol{x}}^{\alpha\beta} - \frac{\delta^{\alpha\beta}}{N_f}, \qquad (19)$$

and, more specifically, on some renormalization group (RG)-invariant quantities associated to this operator. Starting from the two-point correlation function

$$G(\boldsymbol{x} - \boldsymbol{y}) = \langle \mathrm{Tr} Q_{\boldsymbol{x}} Q_{\boldsymbol{y}} \rangle, \qquad (20)$$

we can define the second-moment correlation length

$$\xi^2 = \frac{1}{4\sin^2(\pi/L)} \frac{\widetilde{G}(\boldsymbol{0}) - \widetilde{G}(\boldsymbol{p}_m)}{\widetilde{G}(\boldsymbol{p}_m)}, \qquad (21)$$
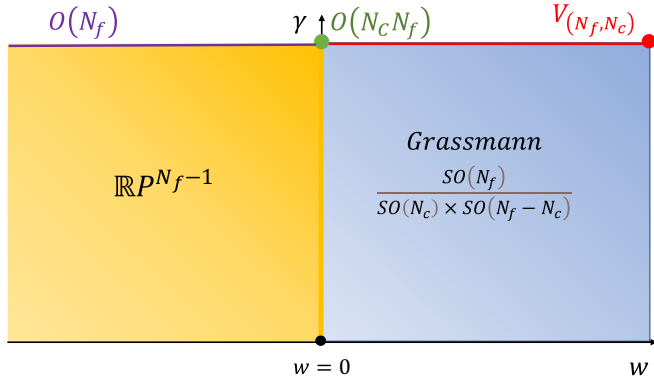
FIG. 1. Graphical representation of the different low-temperature continuum limits expected from the study of the minimum-energy configurations when $N_f > N_c$. Minima of type (i) ($w < 0$) and type (ii) ($w > 0$) are associated to the $\mathbb{R}P^{N_f-1}$ and Grassmannian models, respectively. The case $w = 0$ is numerically found to have the same asymptotic behavior of the $w < 0$ cases (see Ref. [11]). For $\gamma \to +\infty$ we recover the $O(N_f)$ vector model when $w < 0$, the $O(N_cN_f)$ vector model when $w = 0$, and the Stiefel model $V_{(N_f,N_c)}$ when $w > 0$. If $N_f \leqslant N_c$ no critical behavior is expected for $w > 0$

where $\widetilde{G}(\boldsymbol{p}) = \sum_{\boldsymbol{x}} e^{i\boldsymbol{p}\boldsymbol{x}} G(\boldsymbol{x})$ is the Fourier transform of $G(\boldsymbol{x})$ and $\boldsymbol{p}_m = (2\pi/L, 0)$ is the minimum momentum on the lattice. The first RG-invariant quantity we consider is the ratio between the second-moment correlation length and the lattice size,

$$R_\xi \equiv \xi/L, \qquad (22)$$

and lattices with equal extent along the two directions will always be adopted. The second RG-invariant quantity we use is the quartic Binder cumulant U, defined by

$$U = \frac{\langle \mu_2^2 \rangle}{\langle \mu_2 \rangle^2}, \qquad \mu_2 = \frac{1}{L^4} \sum_{\boldsymbol{x},\boldsymbol{y}} \mathrm{Tr} Q_{\boldsymbol{x}} Q_{\boldsymbol{y}}. \qquad (23)$$

Since R_ξ is found to be a monotonic function of the temperature, it is convenient to use R_ξ instead of β to parametrize the Binder cumulant U, writing $U(\beta, L) = U(R_\xi, L)$. Indeed, since both R_ξ and U are RG-invariant quantities, the curve $U(R_\xi, L)$ is expected to approach in the FSS limit (i.e., for $L \to \infty$ at fixed R_ξ) a universal scaling curve

$$U(R_\xi, L) \xrightarrow{\mathrm{FSS}} \mathcal{U}(R_\xi), \qquad (24)$$

where $\mathcal{U}(R_\xi)$ depends on the universality class of the transition, the lattice boundary conditions, and aspect ratio. Scaling corrections of the form $L^{-2} \log^p L$ are expected, as for all asymptotically free theories (see, e.g., Ref. [34] for a detailed analysis of the O(N) models).

In the next section we will use Eq. (24) to investigate whether two different lattice systems share the same universality class. We will also present some numerical results obtained for the Stiefel models in Eq. (17). The observables used for the Stiefel models can be obtained from the ones defined in this section by the replacement $\Phi_{\boldsymbol{x}} \to \pi_{\boldsymbol{x}}/\sqrt{N_c}$.
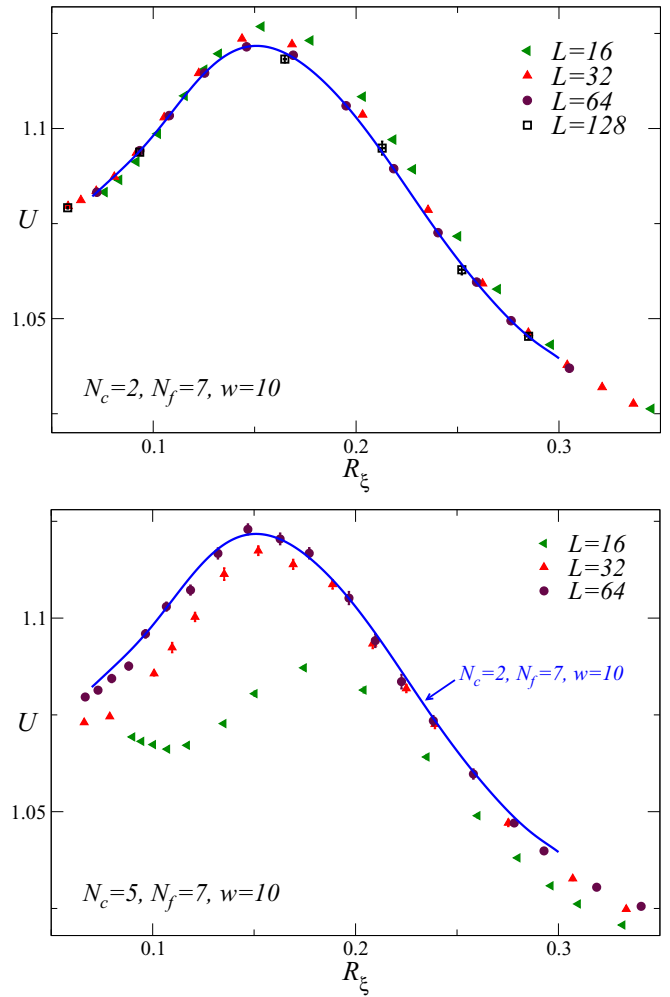

FIG. 2. Top: Binder cumulant U versus R_ξ for the case $N_c = 2$, $N_f = 7$ and quartic coupling $w = 10$ ($\gamma = 0$). The solid line is a polynomial interpolation of the $L = 64$ and $L = 128$ data, and it is our estimate of the asymptotic curve $\mathcal{U}(R_\xi)$ for the Grassmannian SO(7)/(SO(2) × SO(5)) (note that $L = 64$ and $L = 128$ data are consistent with each other). Bottom: Binder cumulant U versus R_ξ for the case $N_c = 5$, $N_f = 7$ and quartic coupling $w = 10$ ($\gamma = 0$). The solid line is the estimate of $\mathcal{U}(R_\xi)$ obtained from $N_c = 2$ data.

V. NUMERICAL RESULTS

In this section we discuss the numerical results obtained by simulating the model defined in Eq. (2). We carried out Monte Carlo simulations and FSS analyses for fixed $N_f = 7$ and several values of N_c, to check the emergence of the color-flavor reflection symmetry $N_c \leftrightarrow N_f - N_c$ in the asymptotic low-temperature critical behavior when $w > 0$. Technical details concerning Monte Carlo simulations are postponed to the Appendix.

In Fig. 2 we present our results for $U(R_\xi, L)$ in the models with $N_c = 2$ and $N_c = 5$, with quartic coupling fixed to $w = 10$ and $\gamma = 0$. For $N_c = 2$ we observe that FSS corrections are quite small, and results coming from lattice sizes $L = 64$ and $L = 128$ are consistent with each other. We thus used a polynomial interpolation of $L = 64$ and 128 data to estimate the universal scaling curve $\mathcal{U}(R_\xi)$ of this model. This universal
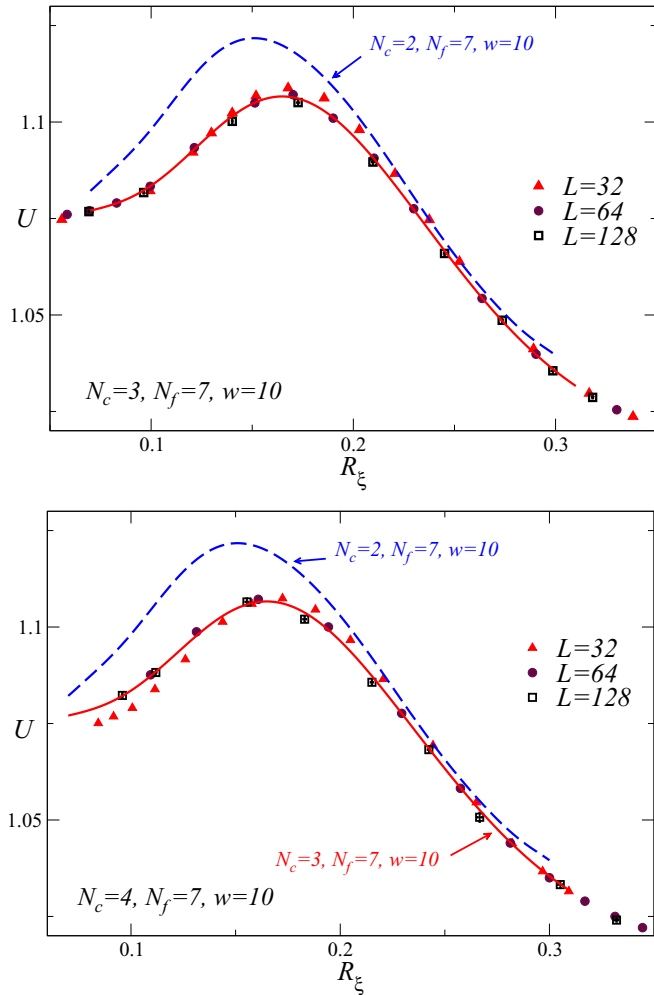
FIG. 3. Top: Binder cumulant U versus R_ξ for the case $N_c = 3$, $N_f = 7$ and quartic coupling $w = 10$ ($\gamma = 0$). The solid line is a polynomial interpolation of the $L = 64$ and $L = 128$ data. The dashed line is our estimate of $\mathcal{U}(R_\xi)$ for the $N_c = 2$, $N_f = 7$ model. Bottom: Binder cumulant U versus R_ξ for the case $N_c = 4$, $N_f = 7$ and quartic coupling $w = 10$ ($\gamma = 0$). The solid line is our estimate of $\mathcal{U}(R_\xi)$ for the $N_c = 3$, $N_f = 7$ model.

curve is then compared, in the bottom panel of Fig. 2, with the results obtained for the $N_c = 5$ model. In this case we observe scaling corrections larger than the ones obtained for $N_c = 2$; however, data for the model with $N_c = 5$ are clearly converging to the same asymptotic curve as the $N_c = 2$ model. The different approaches to the asymptotic curve observed for $N_c = 2$ and $N_c = 5$ show that color-reflection symmetry is not a generic symmetry of the model, but an emerging symmetry in the critical domain.

In Fig. 3 we report data for $U(R_\xi, L)$ in the models with $N_c = 3$ and $N_c = 4$, still with quartic coupling $w = 10$ and $\gamma = 0$. We can immediately note that the critical behavior found in this case is different from the one observed when $N_c = 2$ (and $N_c = 5$), whose universal curve $\mathcal{U}(R_\xi)$ is represented in Fig. 3 by the blue dashed curve. This fact provides an indication that color degrees of freedom actively participate to the critical behavior when $w > 0$. We remind the reader that a completely different behavior was found in Ref. [11]
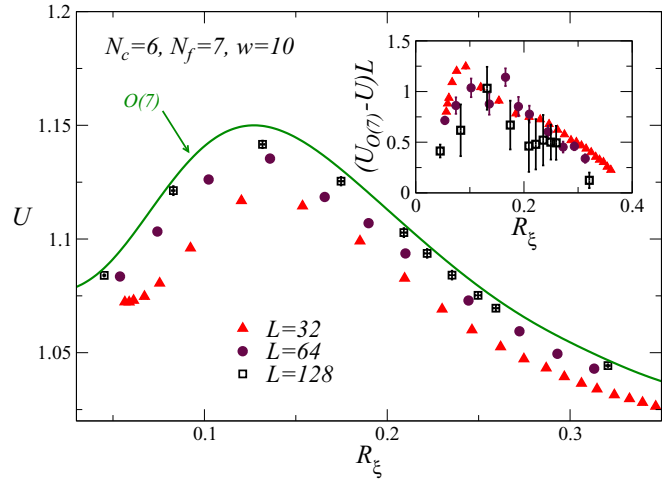

FIG. 4. Binder cumulant U versus R_ξ for the case $N_c = 6$, $N_f = 7$ and quartic coupling $w = 10$ ($\gamma = 0$). For reference we also report our estimate of $\mathcal{U}(R_\xi)$ for spin-2 observables in the vector O(7) model, obtained by a polynomial interpolation of data coming from $L = 32$ and $L = 64$ lattices (consistent with each other within statistical uncertainties). In the inset, scaling corrections are shown to be roughly consistent with an L^{-1} behavior.

for $w = 0$. In that case the low-temperature critical behavior was the same as the $\mathbb{R}P^{N_f - 1}$ model for all the values $N_c > 2$ studied. As discussed in Sec. III the same is expected to happen for negative values of the quartic coupling for any N_c.

We have thus seen that color-reflection symmetry is realized for $N_c = 2$ and 5, and that this symmetry is not trivially realized in the low-temperature phase (i.e., there is a dependence of the critical behavior on N_c). The same procedure adopted to compare the results obtained for $N_c = 2$ and $N_c = 5$ can now be applied to analyze also the cases $N_c = 3$ and $N_c = 4$. The red solid curves in Fig. 3 are obtained by polynomially interpolating data corresponding to $L = 64$ and 128 with $N_c = 3$ (residual corrections to scaling are visible between $L = 64$ and 128, but they are smaller than two standard deviations). The same curve is seen to consistently describe the critical behavior of the model also for $N_c = 4$, as expected on the basis of the emergent color-reflection symmetry.

Finally, in Fig. 4, we discuss the extreme cases $N_c = 1$ and $N_c = 6$, once again for $w = 10$ and $\gamma = 0$. For $N_c = 1$ the model studied reduces to the standard O(7) model (although we use spin-2 observables instead of the usual vector ones), and again an emergent color-flavor reflection symmetry is observed: despite the presence of large scaling corrections, the critical behavior of $U(R_\xi, L)$ for the model with $N_c = 6$ is compatible with the one observed in the O(7) model. As often happens for O(N) models, corrections to scaling are roughly compatible with an L^{-1} scaling [35]. The peak value of the Binder cumulant ($U_{\max} \approx 1.15$) is already sufficient to show that this critical behavior is different from the one seen for $N_c = 2$ ($U_{\max} \approx 1.125$) and $N_c = 3$ ($U_{\max} \approx 1.10$).

We finally want to provide some indication that, for large values of γ, data can be significantly affected by the crossover between the Stiefel and the Grassmanian critical behaviors, with color-flavor reflection symmetry that is absent in the Stiefel case. For this purpose we have first of all determined
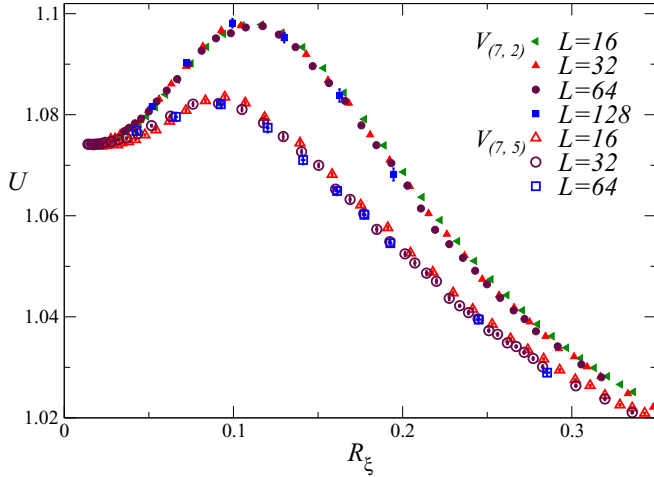
FIG. 5. Binder cumulant U versus R_ξ for the Stiefel models $V_{(7,2)}$ and $V_{(7,5)}$.

the scaling curves $\mathcal{U}(R_\xi)$ for the Stiefel models $V_{(7,2)}$ and $V_{(7,5)}$, shown in Fig. 5. These curves make evident the fact that the color-reflection symmetry characterizing the critical behavior of the gauge models is not present in the Stiefel case. Data for the gauge model with $N_c = 2$, $N_f = 7$, quartic coupling $w = 20$, and gauge coupling $\gamma = 15$ are reported in Fig. 6, and clearly display a crossover behavior between two different regimes. Results slowly converge to the expected Grassmannian asymptotic curve when increasing the lattice size, but on small lattices they are far from it and quite close to the results of the Stiefel model $V_{(7,2)}$. Note, however, that on a finite lattice the $\gamma \to \infty$ limit of the gauge model does not coincide with the Stiefel model with periodic boundary conditions, due to the presence of nontrivial holonomies (Polyakov loops) that cannot be gauged away. To obtain an exact matching one should generalize to the non-Abelian case
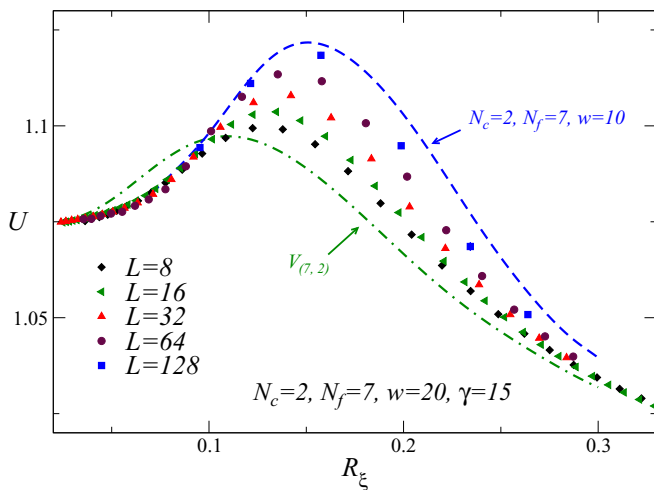

FIG. 6. Binder cumulant U versus R_ξ for the case $N_c = 2$, $N_f = 7$, quartic coupling $w = 20$, and gauge coupling $\gamma = 15$. The dashed line represents our estimate of $\mathcal{U}(R_\xi)$ for the model with $N_c = 2$, $N_f = 7$, $w = 10$, and $\gamma = 0$, while the dot-dashed line is an estimate of $\mathcal{U}(R_\xi)$ for the Stiefel model $V_{(7,2)}$.

the fluctuating boundary conditions used in Ref. [24] for the Abelian case.

VI. CONCLUSIONS

In this paper we have addressed the interplay of local and global symmetries in determining the universal low-temperature critical behavior of two-dimensional (2D) scalar models. In particular, we have considered multiflavor lattice models with $SO(N_c)$ gauge symmetry and non-Abelian $O(N_f)$ global symmetry, in the presence of a quartic interaction between the scalar fields, thus extending the results already presented in Ref. [11].

By studying the minimum-energy configurations, we identified two different low-temperature regimes. If the coefficient of the quartic coupling is negative ($w < 0$), the $SO(N_c)$-gauge models share the same low-temperature critical behavior of the $\mathbb{R}P^{N_f-1}$ models, and color degrees of freedom do not play any active role in the critical domain. In particular the low-temperature effective theory is independent of the number of colors, N_c. If instead $w > 0$, the nature of the low-temperature regime crucially depends on the number of colors and flavors. If $N_f \leqslant N_c$ no global symmetry remains, and no diverging correlation length and critical behavior are present. If instead $N_f > N_c$, the low-temperature behavior is expected to be described by the gauged nonlinear σ model field theory associated with the real Grassmannian manifold $SO(N_f)/(SO(N_c) \times SO(N_f - N_c))$.

To support the identification with the Grassmannian NLσM field theory of the critical behavior when $N_f > N_c$ and $w > 0$, we investigated the N_c dependence of the asymptotic scaling curve $\mathcal{U}(R_\xi)$ and, in particular, the presence of the color-flavor reflection symmetry $N_c \leftrightarrow N_f - N_c$ in the critical region. For this purpose we focused on the case $N_f = 7$, studied for several values of N_c with $w = 10$ and $\gamma = 0$. We numerically verified that gauge degrees of freedom do play a role in the critical behavior, since the asymptotic scaling curves obtained in the cases $N_c = 1$, 2, and 3 are different from each other. Moreover, we provided robust evidence of the emergence of color-reflection symmetry in the critical domain, with the results obtained using N_c and $N_f - N_c$ colors that approach the same asymptotic curve in the FSS limit.

It is interesting to note that for some values of N_c and N_f the Grassmannian models can have peculiar properties that will be worth investigating. For example, the $N_c = 2$ model admits instanton solutions analogous to that of the $\mathbb{C}P^{N-1}$ models, a fact already noted in the seminal work of Ref. [36]. However, to our knowledge the θ dependence of this model has never been systematically investigated.

Another aspect that deserves to be further explored is the stability of the results presented in this paper against an explicit breaking of the gauge symmetry. It is tempting to guess a gauge-breaking term to be relevant for $w > 0$ and irrelevant for $w < 0$, based on the analogy with the case of three-dimensional (3D) Abelian models with critical [37] or noncritical [38] gauge modes. It is, however, not clear *a priori* how far this analogy can be trusted, also because in a non-Abelian theory we have much more freedom on the form of the gauge-symmetry-breaking term, that could, for example, leave a residual continuous subgroup exact.

Finally, in this work we focused on real scalar models with orthogonal gauge symmetry, but an extension to the case of complex scalar models with unitary symmetry can be immediately carried out. In this latter case we can have, depending on the sign of the quartic interaction, a $\mathbb{C}P^{N_f-1}$ critical behavior (for $w < 0$) or a complex Grassmannian $SU(N_f)/(SU(N_c) \times SU(N_f - N_c))$ critical behavior (for $w > 0$).

ACKNOWLEDGMENTS

APPENDIX: MONTE CARLO SIMULATIONS

In this Appendix we present some technical details regarding our Monte Carlo simulations, the algorithms adopted, and the statistics accumulated.

For the gauge models the typical statistics used is of the order of 10^7 "complete lattice sweeps" (defined in the following section), while for the Stiefel models it is of the order of 10^6 complete lattice sweeps. To analyze data and estimate error bars we used standard blocking and jackknife techniques, and the maximum blocking size adopted was of the order of 10^5 and 10^4 data, for gauge and Stiefel models, respectively.

For lattice models with local gauge symmetry, we observed that the value of the inverse temperature β has to be increased to keep R_ξ constant while increasing the value of N_c (at fixed $N_f = 7$). Specifically, for the lattice size $L = 128$, we used for the model with $N_c = 2$ inverse temperatures in the range $\beta \in [1.7, 2.1]$, for $N_c = 3$ we used $\beta \in [3.0, 3.5]$, and for $N_c = 4$ we used $\beta \in [4.5, 5.0]$, while for the case $N_c = 6$ the range $\beta \in [7.5, 8.3]$ was adopted. For the case $N_c = 5$ our largest lattice was $L = 64$, and in this case we used $\beta \in [5.8, 6.3]$. Using these inverse temperature intervals we got values of R_ξ in the range [0.05,0.3] in all the cases.

1. Algorithms: Gauge models

To update the field Φ_x of the gauge models we use both a Metropolis [39] and a pseudo-over-relaxation algorithm [40,41]. In the Metropolis update, the trial field Φ_x' is generated from Φ_x by rotating two random matrix elements by an angle drawn from a uniform distribution in $[-\alpha, \alpha]$. The value of α is chosen in such a way to have an average acceptance rate of about 30%. The pseudo-over-relaxation step is performed by using as a trial field the reflection of Φ_x with respect to the force F_x defined by

$$F_x \equiv \sum_\mu (U_{x,\mu} \Phi_{x+\mu} + U_{x-\mu,\mu}^t \Phi_{x-\mu}), \tag{A1}$$

thus

$$\Phi_x' = \frac{2\mathrm{Tr}(\Phi_x^t F_x)}{\mathrm{Tr}(F_x^t F_x)} F_x - \Phi_x. \tag{A2}$$

This trial field is then accepted or rejected by a Metropolis test, which is unnecessary when $w = 0$ since in that case the update is energy preserving.

The gauge field $U_{x,\mu}$ is updated using the Metropolis algorithm, with the trial link $U_{x,\mu}'$ generated by applying to $U_{x,\mu}$ a random SO(2) matrix randomly embedded in SO(N_c). Also in this case the parameters of the rotation are tuned in order to maintain an average acceptance of approximately 30%.

A "complete lattice sweep" is defined to be a series of ten update sweeps on the whole lattice for both scalar and gauge fields. For the gauge field the Metropolis update is always adopted, while for the scalar field a single Metropolis update is followed by nine pseudo-over-relaxation steps.

2. Algorithms: Stiefel models

The Stiefel Hamiltonian is defined in Eq. (17) by using the field π_x, which is an $N_c \times N_f$ matrix subject to the constraint $\pi_x \pi_x^t = \mathbb{1}_{N_c \times N_c}$. Assuming for the sake of simplicity that $N_f > N_c$, we represent π_x by the first N_c rows of the $N_f \times N_f$ orthogonal matrix $\widetilde{\pi}_x$; that will be our fundamental field in the following. The update of $\widetilde{\pi}_x$ is performed by using the Metropolis algorithm [39] and the single cluster algorithm [42].

The Metropolis update of the field π_x is performed by using the trial state $\widetilde{\pi}_x' = \widetilde{\pi}_x O$, where O is an O(2) random rotation embedded in a random way in O(N_f). The rotation angle is drawn from a uniform distribution in $[-\delta, \delta]$, and the value of δ is chosen to obtain an average acceptance of about 30%.

In the cluster update we start by generating the random unit-length N_f vector v^α and selecting a random lattice site. The cluster construction is performed by activating the link $x - y$ with probability $p_{x,y}$ given by

$$p_{x,y} = 1 - \exp(\min(0, 2\beta N_f X)), \tag{A3}$$

where

$$X = \sum_{i=1}^{N_c} \left[\left(\sum_{\alpha=1}^{N_f} \pi_x^{i\alpha} v^\alpha \right) \left(\sum_{\beta=1}^{N_f} \pi_y^{i\beta} v^\beta \right) \right]. \tag{A4}$$

The whole cluster is then "flipped" using

$$(\widetilde{\pi}_x)^{\alpha\beta} \to (\widetilde{\pi}_x)^{\alpha\beta} - 2v^\beta \sum_{\lambda=1}^{N_f} (\widetilde{\pi}^{\alpha\lambda} v^\lambda), \tag{A5}$$

which is easily seen to be an O(N_f) matrix.

A "complete lattice sweep" is a series of ten Metropolis updates on the whole lattice, each one followed by a cluster update.

[1] S. Weinberg, *The Quantum Theory of Fields* (Cambridge University Press, Cambridge, UK, 2005).

[2] P. W. Anderson, *Basic Notions of Condensed Matter Physics* (Benjamin Cummings, Menlo Park, CA, 1984).

[3] J. Zinn-Justin, *Quantum Field Theory and Critical Phenomena*, 4th ed. (Clarendon Press, Oxford, UK, 2002).

[4] X.-G. Wen, *Quantum Field Theory of Many-Body Systems: From the Origin of Sound to an Origin of Light and Electrons* (Oxford University Press, Oxford, UK, 2004).

[5] S. Sachdev, Topological order, emergent gauge fields, and Fermi surface reconstruction, Rep. Prog. Phys. **82**, 014001 (2019).

[6] F. Englert and R. Brout, Broken Symmetry and the Mass of Gauge Vector Mesons, Phys. Rev. Lett. **13**, 321 (1964).

[7] P. W. Higgs, Broken Symmetries and the Masses of Gauge Bosons, Phys. Rev. Lett. **13**, 508 (1964).

[8] G. S. Guralnik, C. R. Hagen, and T. W. B. Kibble, Global Conservation Laws and Massless Particles, Phys. Rev. Lett. **13**, 585 (1964).

[9] R. D. Pisarski and F. Wilczek, Remarks on the chiral phase transition in chromodynamics, Phys. Rev. D **29**, 338 (1984).

[10] M. Alford, K. Rajagopal, and F. Wilczeck, Color-flavor locking and chiral symmetry breaking in high density QCD, Nucl. Phys. B **537**, 443 (1999).

[11] C. Bonati, A. Franchi, A. Pelissetto, and E. Vicari, Asymptotic low-temperature critical behavior of two-dimensional multiflavor lattice $SO(N_c)$ gauge theories, Phys. Rev. D **102**, 034512 (2020).

[12] C. Bonati, A. Franchi, A. Pelissetto, and E. Vicari, Berezinskii-Kosterlitz-Thouless transitions in two-dimensional lattice $SO(N_c)$ gauge theories with two scalar flavors, Phys. Rev. D **103**, 014510 (2021).

[13] C. Bonati, A. Pelissetto, and E. Vicari, Universal low-temperature behavior of two-dimensional lattice scalar chromodynamics, Phys. Rev. D **101**, 054503 (2020).

[14] C. Bonati, A. Franchi, A. Pelissetto, and E. Vicari, Two-dimensional lattice $SU(N_c)$ gauge theories with multiflavor adjoint scalar fields, J. High Energy Phys. 05 (2021) 018.

[15] N. D. Mermin and H. Wagner, Absence of Ferromagnetism or Antiferromagnetism in One- or Two-Dimensional Isotropic Heisenberg Models, Phys. Rev. Lett. **17**, 1133 (1966).

[16] S. Sachdev, H. D. Scammell, M. S. Scheurer, and G. Tarnopolsky, Gauge theory for the cuprates near optimal doping, Phys. Rev. B **99**, 054516 (2019).

[17] H. D. Scammell, K. Patekar, M. S. Scheurer, and S. Sachdev, Phases of SU(2) gauge theory with multiple adjoint Higgs fields in $2 + 1$ dimensions, Phys. Rev. B **101**, 205124 (2020).

[18] C. Bonati, A. Franchi, A. Pelissetto, and E. Vicari, Phase diagram and Higgs phases of three-dimensional lattice $SU(N_c)$ gauge theories with multiparameter scalar potentials, Phys. Rev. E **104**, 064111 (2021).

[19] K. G. Wilson, Confinement of quarks, Phys. Rev. D **10**, 2445 (1974).

[20] C. Bonati, A. Pelissetto, and E. Vicari, Three-dimensional phase transitions in multiflavor lattice scalar $SO(N_c)$ gauge theories, Phys. Rev. E **101**, 062105 (2020).

[21] G. Zumbach, Phase transitions with $O(n)$ symmetry broken down to $O(n - p)$, Nucl. Phys. B **413**, 771 (1994).

[22] H. Kunz and G. Zumbach, Stiefel models of frustrated antiferromagnets, J. Phys. A: Math. Gen. **26**, 3121 (1993).

[23] D. Loison, Phase transitions in generalized chiral or Stiefel's models, Eur. Phys. J. B **15**, 517 (2000).

[24] C. Bonati, A. Franchi, A. Pelissetto, and E. Vicari, Asymptotic low-temperature behavior of two-dimensional RP^{N-1} models, Phys. Rev. D **102**, 034513 (2020).

[25] M. Hasenbusch, $O(N)$ and RP^{N-1} models in two dimensions, Phys. Rev. D **53**, 3445 (1996).

[26] F. Niedermayer, P. Weisz, and D.-S. Shin, Question of universality in RP^{N-1} and $O(N)$ lattice σ models, Phys. Rev. D **53**, 5918 (1996).

[27] S. M. Catterall, M. Hasenbusch, R. R. Horgan, and R. Renken, Nature of the continuum limit in the 2D RP^2 gauge model, Phys. Rev. D **58**, 074510 (1998).

[28] R. D. Pisarski, Nonlinear σ models of symmetric spaces, Phys. Rev. D **20**, 3358 (1979).

[29] E. Brezin, S. Hikami, and J. Zinn-Justin, Generalized nonlinear Σ models with gauge invariance, Nucl. Phys. B **165**, 528 (1980).

[30] F. Wegner, Four loop order beta function of nonlinear σ models in symmetric spaces, Nucl. Phys. B **316**, 663 (1989).

[31] M. E. Fisher and M. N. Barber, Scaling Theory for Finite-Size Effects in the Critical Region, Phys. Rev. Lett. **28**, 1516 (1972).

[32] *Finite Size Scaling and Numerical Simulation of Statistical Systems*, edited by V. Privman (World Scientific, Singapore, 1990).

[33] A. Pelissetto and E. Vicari, Critical phenomena and renormalization group theory, Phys. Rep. **368**, 549 (2002).

[34] S. Caracciolo and A. Pelissetto, Corrections to finite-size scaling in the lattice N-vector model for $N = \infty$, Phys. Rev. D **58**, 105007 (1998).

[35] J. Balog, F. Niedermayer and P. Weisz, The puzzle of apparent linear lattice artifacts in the 2D non-linear sigma-model and Symanzik's solution, Nucl. Phys. B **824**, 563 (2010).

[36] A. D'Adda, M. Luscher, and P. Di Vecchia, A $1/n$ expandable series of nonlinear sigma models with instantons, Nucl. Phys. B **146**, 63 (1978).

[37] C. Bonati, A. Pelissetto, and E. Vicari, Lattice gauge theories in the presence of a linear gauge-symmetry breaking, Phys. Rev. E **104**, 014140 (2021).

[38] C. Bonati, A. Pelissetto, and E. Vicari, Breaking of Gauge Symmetry in Lattice Gauge Theories, Phys. Rev. Lett. **127**, 091601 (2021).

[39] N. Metropolis, A. W. Rosenbluth, M. N. Rosenbluth, A. H. Teller, and E. Teller, Equation of state calculations by fast computing machines, J. Chem. Phys. **21**, 1087 (1953).

[40] M. Creutz, Overrelaxation and Monte Carlo simulation, Phys. Rev. D **36**, 515 (1987).

[41] S. L. Adler, An overrelaxation method for the Monte Carlo evaluation of the partition function for multiquadratic actions, Phys. Rev. D **23**, 2901 (1981).

[42] U. Wolff, Collective Monte Carlo Updating for Spin Systems, Phys. Rev. Lett. **62**, 361 (1989).